

Joint inversion of potential-fields data over the DO-27 kimberlite pipe using a Gaussian mixture model prior

Thibaut Astic¹, Dominique Fournier², and Douglas W. Oldenburg¹

Abstract

We have carried out petrophysically and geologically guided inversions (PGIs) to jointly invert airborne and ground-based gravity data and airborne magnetic data to recover a quasi-geology model of the DO-27 kimberlite pipe in the Tli Kwi Cho (also referred to as TKC) cluster. DO-27 is composed of three main kimberlite rock types in contact with each other and embedded in a granitic host rock covered by a thin layer of glacial till. The pyroclastic kimberlite (PK), which is diamondiferous, and the volcanoclastic kimberlite (VK) have anomalously low density, due to their high porosity, and weak magnetic susceptibility. They are indistinguishable from each other based upon their potential-field responses. The hypabyssal kimberlite (HK), which is not diamondiferous, has been identified as highly magnetic and remanent. Quantitative petrophysical signatures for each rock unit are obtained from sample measurements, such as the increasing density of the PK/VK unit with depth and the remanent magnetization of the HK unit, and are represented as a Gaussian mixture model (GMM). This GMM guides the PGI toward generating a 3D quasi-geology model with physical properties that satisfies the geophysical data sets and the petrophysical signatures. Density and magnetization models recovered individually yield volumes that have physical property combinations that do not conform to any known petrophysical characteristics of the rocks in the area. A multiphysics PGI addresses this problem by using the GMM as a coupling term, but it puts a volume of the PK/VK unit at a location that is incompatible with geologic information from drill-holes. To conform to that geologic knowledge, a fourth unit is introduced, PK-minor, which is petrophysically and geographically distinct from the main PK/VK unit. This inversion produces a quasi-geology model that presents good structural locations of the diamondiferous PK unit and can be used to provide a resource estimate or decide the locations of future drillholes.

Introduction and geologic setting

The DO-27 kimberlite pipe is located in the kimberlite-rich Lac De Gras region, Northwest Territories, Canada (Figure 1). It was first discovered in 1992, following the discovery of the Ekati kimberlite field in September 1991 (Kjarsgaard and Levinson, 2002), thanks to an airborne frequency-domain electromagnetic survey (DIGHEM). Two distinct anomalies were identified, which were initially thought to be part of a single large complex. After multiple revisions of the conceptual geologic model (Harder et al., 2009), it is now believed that there are two main pipes, designated as DO-18 and DO-27, with distinct rock types. Kimberlite pipes are potentially diamondiferous, and the assessment of their economic potential requires an understanding of their geologic structures.

Several types of kimberlite facies can reside inside the same pipe. A schematic representation of the architecture of a typical Lac de Gras pipe is shown in

Figure 2a. The various kimberlite facies are classified based on their genesis (Field and Smith, 1998; Kjarsgaard, 2007). At DO-27, there are three main facies embedded in a granitic host rock that play a role in the potential-field responses. The first is a hypabyssal kimberlite (HK), which is an intrusive igneous rock often found at the base of the pipe (Figure 2a). The second is a volcanoclastic kimberlite (VK), which is an extrusive igneous rock with high porosity, which is typically found above the HK unit. The last facies is a pyroclastic kimberlite (PK), which is the diamondiferous unit at DO-27. It shares many characteristics with VK because both formed during extrusion events accompanied by an explosion. Glaciers eroded the top of the pipes, allowing the formation of lakes, and deposited a thin layer of till (Dyke and Prest, 1987; Doyle et al., 1998).

The geologic model of the DO-27 pipe built from several drilling campaigns is presented in Figure 2b. The geometry of DO-27 diverges significantly from the

¹The University of British Columbia, Geophysical Inversion Facility, Department of Earth, Ocean and Atmospheric Sciences, 2020-2207 Main Mall, Vancouver, BC V6T 1Z4, Canada. E-mail: thast@eoas.ubc.ca (corresponding author); doug@eos.ubc.ca.

²Mira Geoscience, 512B-409 Granville Street, Vancouver, BC V6C 1T2, Canada. E-mail: dominiquef@mirageoscience.com.

Manuscript received by the Editor 6 December 2019; revised manuscript received 29 May 2020; published ahead of production 7 July 2020; published online 12 October 2020. This paper appears in *Interpretation*, Vol. 8, No. 4 (November 2020); p. SS47–SS62, 14 FIGS., 2 TABLES.

<http://dx.doi.org/10.1190/INT-2019-0283.1>. © 2020 Society of Exploration Geophysicists and American Association of Petroleum Geologists. All rights reserved.

standard kimberlite model with a sheet-like hypabyssal unit present near the surface. [Harder et al. \(2009\)](#) conclude that DO-27 was formed in several successive volcanic phases with the HK unit predating the VK intrusion ([Doyle et al., 1998](#)). This VK intrusion was later disturbed by another volcanic event, with the PK unit infilling the pipe. Several minor occurrences of kimberlite units identified as PK facies have been observed close to the surface. As discussed in [Devriese et al. \(2017\)](#), the density and magnetic characteristics of the different units are as follows. (1) The PK and VK units have low density and are weakly magnetically susceptible. They are indistin-

guishable from each other in potential-field surveys, and we thus refer to them as a PK/VK unit. (2) The HK unit has a density that is close to the granitic host rock, but it has a high magnetic susceptibility and is remanently magnetized. (3) The thin horizontal layer of glacial till, that only plays a minor role from a potential-field standpoint, and granitic host rock are regrouped under the term “background.”

Geophysics plays an important role in kimberlite exploration ([Macnae, 1995](#); [Keating and Sailhac, 2004](#); [Power and Hildes., 2007](#)), and much work has been done over the DO-27 and DO-18 kimberlite pipes. [Jansen and Witherly \(2004\)](#) present an overview of the exploration geophysical surveys acquired before 2000. [Devriese et al. \(2017\)](#) perform smooth inversions of individual potential-field data sets. Their interpretation of the physical property models defines the overall shape of the DO-27 and DO-18 pipes. Their analysis provides a valuable start in distinguishing between the PK/VK and the HK units. [Fournier et al. \(2017\)](#) focus on the inversion and interpretation of the electromagnetic surveys. They are able to distinguish the top of the pipe from the lake-bottom sediments and till layer. Finally, [Kang et al. \(2017\)](#) extract induced polarization information from airborne electromagnetic surveys to distinguish between adjacent kimberlites based on their clay mineral content. They subsequently build a geologic model using a post-inversion classification. The inputs to their classification were density, magnetic susceptibility, electrical conductivity, and chargeability obtained from the individual smooth inversions.

The use of post-inversion classification to infer geologic information has been widely used, for example, in [Oldenburg et al. \(1997\)](#), [Paasche et al. \(2006\)](#), [Giuseppe et al. \(2014\)](#), [Martinez and Li \(2015\)](#), [Paasche \(2016\)](#), and [Melo et al. \(2017\)](#). However, there are challenges in using this methodology. Geophysical inversion generally produces a smooth image of the earth, and the details are dependent upon parameters in the inversion. Building a geologic model from these inversions also requires specifying thresholds and criteria to discriminate between

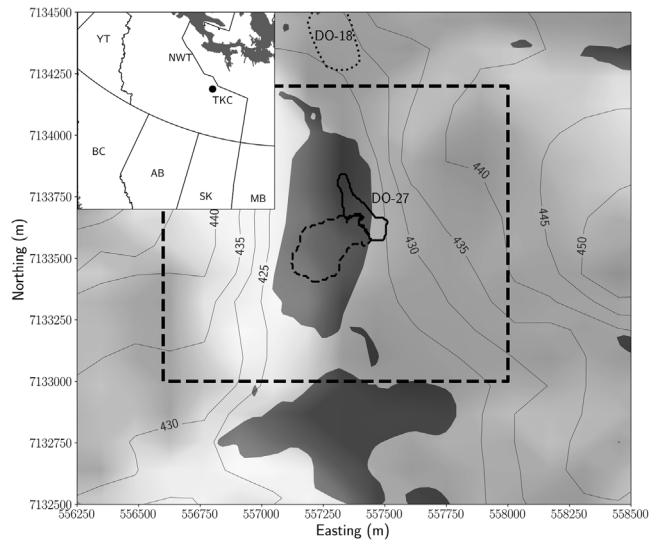


Figure 1. Topography map (contours and shaded background) and hydrography at the DO-27 kimberlite pipe in the Northwest Territories, Canada (location in the inset). The area of interest is represented as a dashed box. Outline of the PK/VK (dashed) and HK (solid) kimberlite facies present in the pipe, extracted from the geologic model at 285 m of elevation, are overlaid on the map. The DO-18 pipe is visible at the northern boundary of the map. Geographic projection: UTM 12N, NAD27.

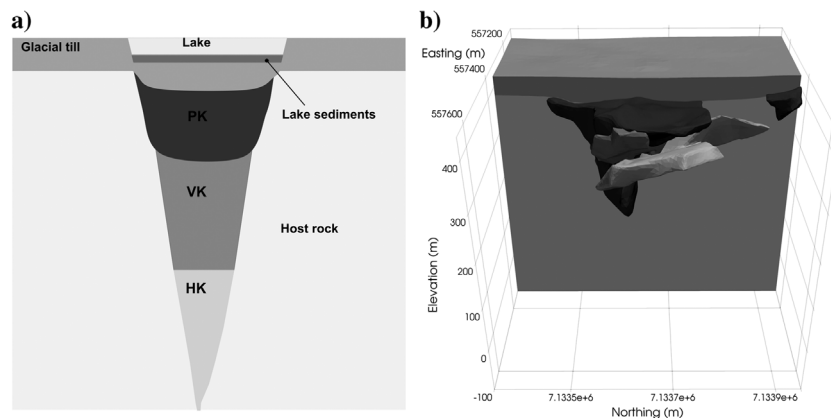


Figure 2. (a) Lac De Gras kimberlite pipe conceptual model (modified from [Devriese et al., 2017](#)). HK: Hypabyssal kimberlite facies; VK: Volcanoclastic kimberlite facies; and PK: Pyroclastic kimberlite facies and (b) current geologic representation of the DO-27 pipe based on drillholes.

rock units; these are subjective choices and need expert knowledge that can make post-inversion classification challenging for problems such as resource estimation, which for DO-27 is linked to the volume of the PK/VK unit. Rather than generate a quasi-geology model from a post-inversion classification ([Li et al., 2019](#)), our goal is to carry out a single inversion that integrates potential-fields data with petrophysical and geologic information. We use a joint inversion framework ([Astic and Oldenburg, 2019](#); [Astic et al., 2020](#)) for petrophysically and geologically guided inversion (PGI). It produces physical property models that fit both the geophysical and petrophysical data, which allows the inversion to build a quasi-geol-

ogy model. In this study, we jointly invert potential-fields data from a ground gravity survey, an airborne gravity gradiometry (Falcon) survey (Lee, 2001), and an airborne magnetic survey (acquired during a versatile time-domain electromagnetic (VTEM) survey; Witherly, 2005). We use the petrophysical signatures of the background, PK/VK, and HK rock units as a coupling term. This coupling term links density, the three components of the magnetization of the rocks, and the elevation to account for variations of the density signature of the PK/VK unit with depth. The petrophysical data are represented as a Gaussian mixture model (GMM) (Dempster et al., 1977; Murphy, 2012). This GMM is used to generate a misfit function that quantifies how well the inversion fits the petrophysical signatures. A successful inversion simultaneously achieves acceptable fits of the geophysical and petrophysical data.

This study is segmented into five parts. First, we introduce the geophysical data sets and our data processing steps. We then summarize our PGI methodology for representing petrophysical and geologic information and how to include it in an inversion. Next, we design the GMM from the available petrophysical data by identifying the physical properties characteristics of each rock unit. Our first inversion with the PGI approach focuses on recovering density from the two gravity surveys. We jointly invert ground gravity and Falcon data to recover a density model that is consistent with the PK/VK density increase with depth. We then invert the magnetic data from the VTEM survey. To recover a magnetization model consistent with the high remanence of the HK unit, we use a magnetic vector inversion (MVI). We show that combining these density and magnetic vector models yields volumes with erroneous combinations of physical properties and uncertainties about the extent of the HK and PK/VK units. We follow up with a fully integrated multiphysics inversion of the potential-field data sets by inverting all three geophysical surveys together with the signature of all three rock units (background, PK/VK, and HK). This model is a significant improvement over what is obtained from post-inversion classifications. The delineation of the diamondiferous PK/VK unit over the central part of the DO-27 pipe is in good agreement with the outline drawn from drillholes. However, the model disagrees with drill-hole information north of the DO-27 pipe. To address this, we add to our inversion geologic information from drillholes and an extra rock unit to represent minor near-surface occurrences of PK facies. The final quasi-geology model obtained with our PGI approach resolves the geologic conflicts and allows us to estimate the volume of the PK/VK unit, which is the potential diamondiferous resource at DO-27.

Geophysical data sets

Ground gravity

Ground gravity data were acquired, on the ice, over DO-27 in the spring of 1994. The survey is composed of 441 stations with spacing of 25 m along east–west lines 100 m apart. Gravity data were processed by the contractor and provided as the complete Bouguer anomaly.

In preparation for the inversion, we upward continued the data by 6.25 m so that they are a half cell width above the surface. This is done to minimize the effects of potential small-scale heterogeneities inside a subsurface cell that is mathematically modeled as a volume with homogeneous density (Li and Oldenburg, 1996). A low-frequency signal was seen in our early inversions that manifested as density contrasts in the padding cells. Although this low-frequency signal can be absorbed this way, we chose to remove a linear trend from the data to focus the inversion on the local anomalies. We use a robust Cauchy loss function for the linear regression, which is less affected by outliers than a least-squares estimation (Kadiyala and Murthy, 1977). The processed data set is shown in Figure 3b.

A clear negative anomaly of -2.14 mGal, associated with the DO-27 kimberlite pipe, is visible. A northern extension was first interpreted as a connection between the DO-18 and the DO-27 kimberlite pipes. The current understanding is that it is due to several minor near-surface kimberlite dikes and sills (Doyle et al., 1998).

In the inversion, we assign a uniform unbiased Gaussian noise level with a standard deviation of 0.045 mGal; this is identical to what is used in Devriese et al. (2017).

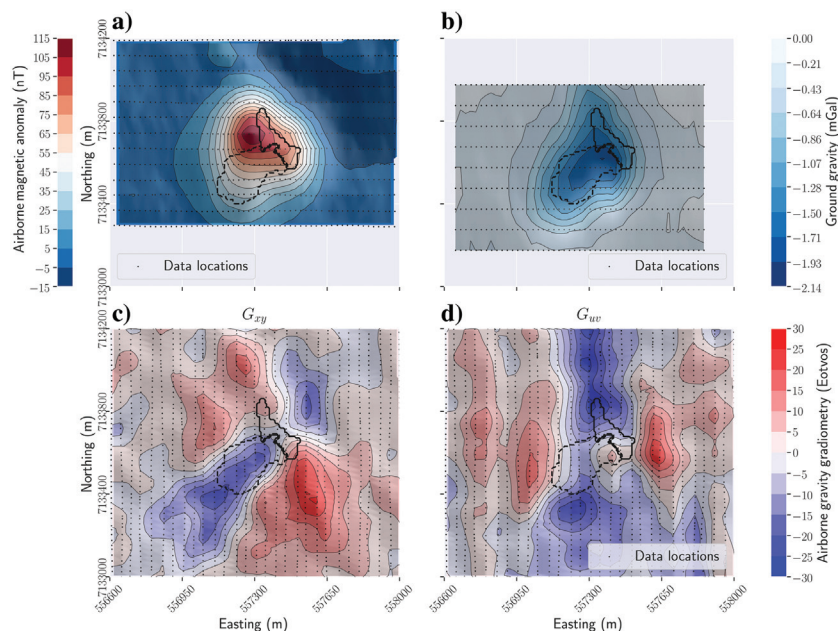


Figure 3. Four potential-field data sets, collected over the DO-27 pipe, which are used in this study (after regional removal). (a) Airborne VTEM total field magnetic survey, (b) ground gravity survey, (c) G_{xy} component of the airborne Falcon gravity gradiometry survey, and (d) the G_{uv} component of the airborne Falcon gravity gradiometry survey.

Falcon airborne gravity gradiometry

An airborne Falcon gravity gradiometry survey was flown in 2001 over the property. Over the area of interest, the survey flew 29 north–south flight lines spaced 50 m apart with an average 53 m ground clearance. We downsampled the data along the lines to one measurement every 25 m to yield approximately one data point per surface cell in our mesh. This ensures that there is no signal in the data with a smaller wavelength than can be modeled by the mesh (Figure 3c and 3d).

At each station, two combinations of the gravity gradiometry tensor (Pawłowski, 1998) are measured by the Falcon system (Lee, 2001). The first component is G_{xy} . The second measurement is a linear combination of two components of the tensor: $G_{uv} = (G_{yy} - G_{xx})/2$. We invert directly for those two measurements. The data were processed by the contractor with an equivalent source transformation using a 2.67 g/cm^3 background density.

In the inversion, we assign a uniform unbiased Gaussian noise level with a standard deviation of five eotvos for G_{xy} and G_{uv} components; this is identical to the one used in Devriese et al. (2017).

Airborne magnetic survey

Total field magnetic data were recorded during a VTEM survey flown in 2004 over the property, using a cesium vapor magnetometer towed 15 m below the aircraft. The survey over the area of interest is composed of 13 east–west flight lines 75 m apart at an average 72 m ground clearance.

Before the inversion, we removed a linear trend from the data using a Cauchy norm. We downsampled the lines to one data point every 25 m. The processed data set is shown in Figure 3a.

A strong positive anomaly of 115 nT is visible north of the complex. It is associated with a negative signal of

–15 nT on the northeast; this is relatively strong for that latitude. It suggests that the data are affected by a strong remanent magnetization (Devriese et al., 2017).

To handle the different types of magnetization (induced and remanent) and the uncertainties about the remanent field direction (see Devriese et al., 2017; and the section below about modeling the petrophysical information), we use a full MVI with a Cartesian formulation (Lelièvre and Oldenburg, 2009) to invert the magnetic data.

In the inversion, we assign a uniform unbiased Gaussian noise level with a standard deviation of 1 nT; this is identical to the noise level used in Devriese et al. (2017).

Inversion methodology

The geophysical inverse problem

In our PGI approach, each iteration is similar to a smooth inversion (Oldenburg and Li, 2005) that minimizes an objective function Φ

$$\underset{\mathbf{m}}{\text{minimize}} \Phi(\mathbf{m}) = \Phi_d(\mathbf{m}) + \beta\Phi_m(\mathbf{m}), \quad (1)$$

where \mathbf{m} is our geophysical model, which represents the physical properties on a mesh. The term Φ_d contains the sum of the various geophysical data misfits. The term Φ_m is the model regularization. The parameter β is a positive scalar that balances the two terms.

The regularization is divided into two main terms: the smallness, which measures the distance to a reference model, and the smoothness, which regulates the variations of the model in each direction:

$$\Phi_m(\mathbf{m}) = \alpha_s \underbrace{\Phi_s(\mathbf{m})}_{\text{smallness}} + \sum_{i \in \{x,y,z\}} \alpha_i \underbrace{\Phi_i(\mathbf{m})}_{\text{smoothness}}. \quad (2)$$

All of the inversions presented here are carried out with the open-source SimPEG package (Cockett et al., 2015). In addition, they all share the same octree mesh (Figure 4). The use of an octree mesh significantly speeds up the inversions while maintaining high resolution in the area of interest. All of the inversions start from null half-space initial and reference models. For all of the joint inversions, we use the computationally inexpensive strategy outline in Astic et al. (2020) to handle multiple geophysical surveys, where the weights of the components of the total data misfit term are adjusted during the inversion until each geophysical misfit is equal or below its target value (Parker, 1977).

Smooth inversions of all of the individual potential-field surveys can be found in Devriese et al. (2017). To extend that work, and to highlight the gains obtained using a PGI approach, we show two additional smooth inversion results: a smooth

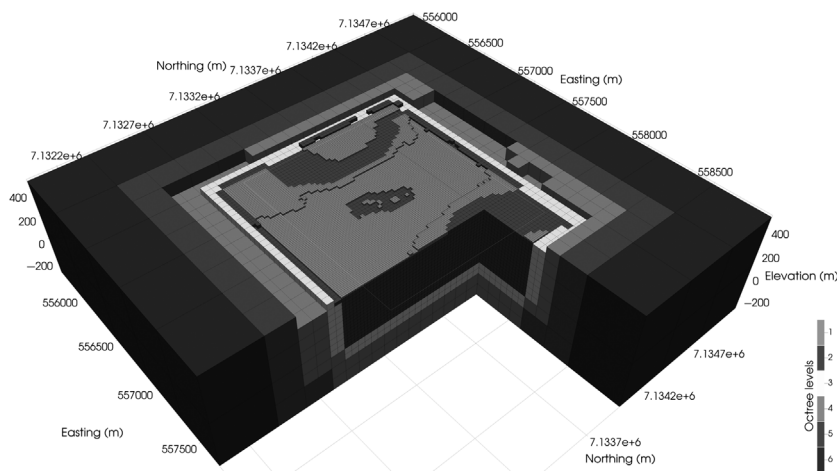


Figure 4. The octree mesh used for all of the inversions. The area of interest is outlined in white. The octree levels represent each increase in cell size (with level 1 being the smallest cells). The volume of interest is discretized with 25 m cubic cells (level 2). The topography is accommodated with a layer of the smallest cells (12.5 m cubic cells, level 1). The other levels (three and more) serve as padding.

inversion combining the gravity and gravity gradiometry data and a smooth MVI of the magnetic data. A post-inversion combination of the physical property models is then conducted (Figure 5).

We first perform the smooth joint inversion of the ground gravity and Falcon gravity gradiometry surveys. This is possible because both surveys are sensitive to the same physical property. The plan view and cross sections of the recovered density model are shown in Figure 5a. The model is relatively smooth, as is expected, and the low-density material extends well beyond the boundaries of the outline of the kimberlite units.

We then carry out the unconstrained smooth MVI to recover the magnetization vector for each cell. The MVI problem is more challenging than gravity inversions because three components need to be recovered. We use the Cartesian approach outlined in Lelièvre and Oldenburg (2009) and find a smooth solution for each component. The plan view and cross sections of the recovered model are shown in Figure 5b. Each magnetization vector is projected onto the plotting plane. The recovered vector magnetizations smoothly vary in amplitude and orientation, as is expected. Only the large-scale region of high magnetization is predominantly visible. The cross sections chosen for magnetization are not in the same location as those used for density because high magnetizations occur at a different location than the high-density contrast values. It is reflective of the different rock units that are generating the two responses. Close to the location of the HK unit, the vectors are oriented in a direction close to the remanent field direction estimated in Devriese et al. (2017) (inclination: 53° and declination: 22°).

To evaluate the interpretation achievable by combining our smooth inversions, we take the magnitude of the magnetization, convert it to an effective susceptibility, and then we plot the scatterplot of magnetization versus density (Figure 5c). We color the points based on the density contrast and the magnetization strength (shades of blue are for significant density contrast only, red is for magnetic contrast, and purple is when both contrasts occur). The scale is provided in Figure 5d. No distinct clustering of rocks is observed. In Figure 5d, each cell in the model is assigned a color that conveys the relative values of the physical properties in that cell. For instance, a white cell denotes a background rock whereas a blue cell indicates a rock that has low density. Figure 5c and 5d highlights that trying to evaluate a specific volume for the PK/VK unit from these inversions would be highly dependent on the thresh-

old value that one would choose to delineate the body. Estimates obtained with clustering algorithms would have the same issues. Those limitations motivate the search for an improved solution that reproduces the petrophysical characteristics of each rock.

Representing petrophysical and geologic information as a GMM

To include physical property information into the inversion, we model the petrophysical signature of each rock unit by a Gaussian probability distribution. Each unit (indexed j , for a total of c units) is defined by the mean of its physical properties (μ_j) and a covariance matrix linking the various physical properties (Σ_j). Computations of those values based on the samples are shown in equations 3 and 4. Measured physical properties for a sample s belonging to rock unit j is represented by $\mathbf{x}_{s \in j}$. The number of available samples for the rock unit j is denoted as s_j :

$$\mu_j = \frac{1}{s_j} \sum_{s=1}^{s_j} \mathbf{x}_{s \in j}. \quad (3)$$

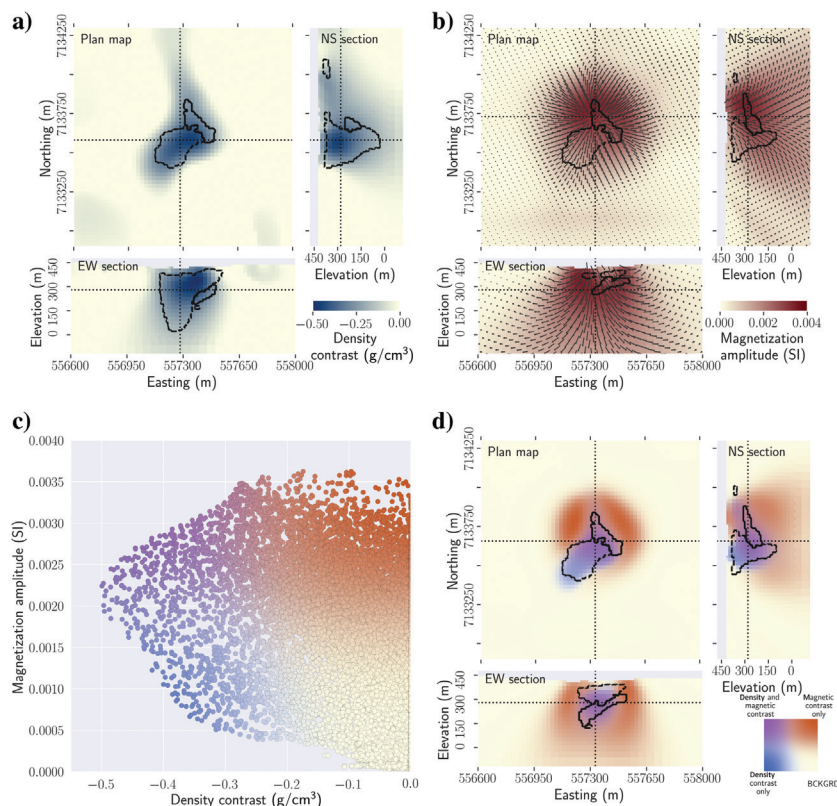


Figure 5. Results of the smooth gravity inversion and MVI and post-inversion analysis. (a) Plan map, east–west, and north–south cross sections through the density model obtained by joint smooth inversion of the ground gravity and Falcon data. The dotted lines represent the location of each cross section; (b) plan map, east–west, and north–south cross sections through the magnetic vector model obtained by MVI of the magnetic data. The dark arrows represent the magnetization direction and strength of the magnetic vector projected on the plane; (c) scatterplot of the inverted density contrast and magnetization strength colored based on the physical properties; and (d) colored model based on the density contrast and magnetization strength couple.

$$\Sigma_j = \frac{1}{s_j} \sum_{s=1}^{s_j} (\mathbf{x}_{s \in j} - \boldsymbol{\mu}_j)(\mathbf{x}_{s \in j} - \boldsymbol{\mu}_j)^T. \quad (4)$$

The Gaussian distribution representing each unit j is denoted as $\mathcal{N}(\cdot | \boldsymbol{\mu}_j, \Sigma_j)$. We regroup the petrophysical and geologic information of all the known units in the form of a GMM (equation 5), which is a sum of the Gaussian signatures weighted by the prior probability of encountering the rock unit j at the location i (denoted $\pi_{i,j}$). This last parameter does not have to be precise and has minimal effects when set constant everywhere. Allowing those probabilities to vary depending on the location provides an additional way to include geologic information (Giraud et al., 2017), and we use this functionality later in this paper. Thus, the probability function to observe a physical properties data point \mathbf{x} at location i can be written as

$$\mathcal{P}(\mathbf{x}_i) = \sum_{j=1}^c \pi_{i,j} \mathcal{N}(\mathbf{x}_i | \boldsymbol{\mu}_j, \Sigma_j). \quad (5)$$

A fictitious example of a GMM with two physical properties (the axes) and two rock units (the Gaussian distributions) is shown in Figure 6. Each Gaussian represents the petrophysical signature of a rock unit for the two physical properties. The background color highlights the most likely rock unit for any given values of the physical properties; we refer to this classification as the geologic identification.

Key concepts for PGI

As put forward in Astic and Oldenburg (2019), we can build upon the objective function in equation 1 to incorporate petrophysical and geologic information (represented as a GMM) to better constrain our physical property models. This prior knowledge is contained within the smallness term (equation 2). The PGI problem is nonlinear, and the objective function is minimized iteratively (Oldenburg and Li, 2005). At each iteration, the reference model \mathbf{m}_{ref} and the smallness weights W_s are updated based on our knowledge of the petrophysical and geologic characteristics. Our augmented smallness term then takes the following form:

$$\Phi_s(\mathbf{m}) = \frac{1}{2} \sum_{i=1}^n \|W_s(z_i)(\mathbf{m}_i - \mathbf{m}_{\text{ref}}(z_i))\|_2^2, \quad (6)$$

with

$$z_i = \operatorname{argmax}_j \pi_{i,j} \mathcal{N}(\mathbf{m}_i | \boldsymbol{\mu}_j, \Sigma_j), \quad (7)$$

$$\mathbf{m}_{\text{ref}}(z_i) = \boldsymbol{\mu}_{z_i}, \quad (8)$$

$$W_s(z_i) = \Sigma_{z_i}^{-1/2} \operatorname{diag}(\mathbf{w}_i), \quad (9)$$

where z_i denotes the geologic identification and \mathbf{w}_i are sensitivity weights for each physical property at cell i , for a total number of n cells. The update can be understood as a classification of each cell of the mesh into its most likely geologic unit based on the current geophysical model and prior knowledge (equation 7). This classification defines our quasi-geology model, and it is used to create a new reference model and smallness weights with the following procedure. For the reference model \mathbf{m}_{ref} , each cell is assigned the petrophysical mean values of the identified rock unit (equation 8). The smallness weights W_s at each cell include the covariance matrix of the physical properties for the identified rock unit to represent the expected variations and correlations (equation 9); they also include the sensitivity weights for each physical property, necessary for potential field inversions (Li and Oldenburg, 1996, 1998; Li, 2005). This iterative update of the smallness term guides the inversion toward reproducing the petrophysical signature of each rock unit while fitting the geophysical data.

Modeling the petrophysical information at DO-27

Qualitative information about the physical properties of the various rock types found at DO-27 was used during previous studies relying on Tikhonov inversions (Devriese et al., 2017; Fournier et al., 2017; Kang et al., 2017). For our work, we need more quantitative information from field samples. We obtained 20 samples of the various kimberlite facies from Peregrine Diamonds Ltd. Eleven samples of PK, four of VK, and five of HK were sent to the Geological Survey of Canada Paleomagnetism and Petrophysics Laboratory, Victoria, BC, for characterizing the physical properties of each unit. In the following material, we discuss those measurements and how we compiled the information into a form that allows us to generate a GMM. Means and standard deviations summarizing the petrophysical characteristics of each rock unit are provided in Table 1.

Density information

The HK samples were mechanically competent, and five densities were obtained: 2.764, 2.867, 2.435, 2.632, and 2.677 g/cm³. Those samples yield an average density of 2.675 g/cm³, which is similar to the estimated background density of 2.67 g/cm³ (Devriese et al., 2017). The HK unit is deemed to be indistinguishable from the background regarding its density standpoint. The mean density contrast of both rock units is thus set to 0 g/cm³. However, the density of the background unit is assigned a smaller standard deviation.

The PK and VK units are highly porous and mechanically weak. Unfortunately, this prevented density information from being obtained from several samples. Those that were successfully analyzed are believed to be associated with more competent and denser samples. Those samples are thus deemed to be unrepresentative of the kimberlite units in general and were not used. Instead, we rely on density measurements

taken by Peregrine Diamonds Ltd. during the drilling programs. A block model of the density of PK was built based on those measurements (Eggleston et al., 2014). To include this information in our inversion, we digitized the published cross section through this block model (Figure 7a). Assuming a background density of 2.67 g/cm^3 , the density contrast is approximately -1.1 g/cm^3 at 400 m elevation and it changes linearly to achieve a value of approximately -0.5 g/cm^3 at 200 m elevation. This cross section provides enough information for us to characterize the density signature of the PK/VK unit and build a GMM. To include the linear trend of density contrast with depth, we add the elevation as a fixed parameter in our coupling term. We generate a 2D GMM (density contrast and elevation) that is consistent with the observations (shown in Figure 7b along with the scatterplot of the cross section). The elongated and tilted shape of the Gaussian distribution representing the PK/VK unit accounts for the correlation of the density contrast with depth. On the contrary, the background (and HK) density values are assumed to be independent of the depth. This is modeled by assigning a high standard deviation for the elevation of those units; their assigned mean elevation then is of no consequence in the inversion. The long vertically elongated shape of the Gaussian distribution for the background unit manifests the independence of the density contrast with respect to the elevation for that unit. Means and standard deviations characterizing the density contrast of each rock unit are provided in Table 1.

Magnetic susceptibility information

For our samples, both the induced magnetization and the strength of the remanent field were measured (Figure 8a). The strength of the remanent field was given in the form of a Koenigsberger ratio (Koenigsberger, 1938). The magnetic susceptibility of the samples spans a wide range of values, which is consistent with the fact that magnetic susceptibility generally has a logarithmic distribution (Latham et al., 1989; Rauen et al., 2000; Enkin et al., 2020).

If we are given the remanent magnetization direction, we can estimate an effective susceptibility k_{eff} for the magnetic vector of each unit:

$$k_{\text{eff}} = k \|\hat{u}_{\text{earth}} + Q \frac{B_{\text{lab}}}{B_{\text{earth}}} \hat{u}_{\text{rem}}\|_2, \quad (10)$$

where k is the measured magnetic susceptibility (the purely inductive magnetic response), \hat{u}_{earth} is the unit vector of the earth's magnetic field direction at DO-27, Q is the Koenigsberger ratio, B_{earth} is the International Geomagnetic Reference Field (IGRF) at DO-27,

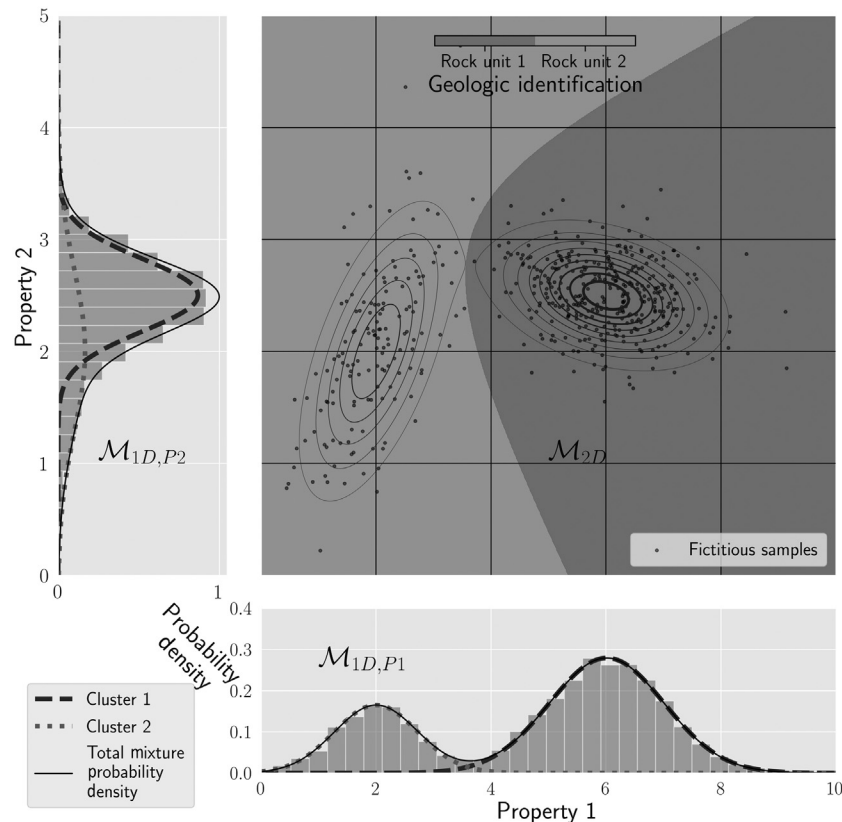


Figure 6. Example of a GMM with two properties (the axes) and two rock units (the Gaussian distributions). The main panel shows the 2D GMM distribution with isoprobability level contour lines: the thicker lines indicate higher probabilities. The background is colored according to the geologic identification prediction. The left and bottom panels show the GMM projections in 1D for each property and the histogram of the fictitious samples. The figure is modified from Astic et al. (2020).

Table 1. Physical properties and elevation parameters for each rock unit. For the PK/VK-pipe unit, the values are reported without the rotation of the Gaussian distribution caused by the linear trend with depth.

| Rock unit | $\bar{\rho}$ | σ_{ρ} | \bar{z} | σ_z | \bar{k} | σ_k | $\bar{\theta}$ | $\bar{\phi}$ | $\sigma_{\theta, \phi}$ |
|------------|--------------|-----------------|-----------|------------|-----------|------------|----------------|--------------|-------------------------|
| Background | 0 | 0.03 | 290 | 180 | -6 | 0.24 | 83.8 | 19.5 | 10 |
| PK/VK | -0.78 | 0.07 | 290 | 75 | -3.1 | 0.24 | 83.8 | 19.5 | 10 |
| HK | 0 | 0.1 | 290 | 180 | -1.3 | 0.33 | 53 | 22 | 10 |
| PK-minor | -0.3 | 0.1 | 360 | 10 | -3.1 | 0.24 | 83.8 | 19.5 | 10 |

Notation and units: \bar{x} is the mean of x , σ_x is the standard deviation of x , ρ is the density contrast (g/cm^3), z is the elevation (m), k is the effective magnetic susceptibility (log 10 SD), θ is the inclination ($^{\circ}$), and ϕ is the declination ($^{\circ}$).

B_{lab} is the amplitude of the magnetic field used in the laboratory for the measurements (59,000 nT), and \hat{u}_{rem} is the unit vector of the remanent magnetization direction.

The PK and VK units have a small magnetic susceptibility and are weakly remanent. The effective susceptibility of those two units, assuming that the remanent field is aligned with the current earth's magnetic field, is estimated at 8×10^{-4} SI.

Only four samples of HK were measured for their magnetic response. Their Koenigsberger ratios are close to 10. Hence, the magnetic response of the HK unit in the data is essentially due to remanent magnetism. However, we need an estimation of the remanent magnetization orientation of the HK unit to obtain an effective susceptibility. Devriese et al. (2017) obtain an estimation of a 53° inclination and 22° declination by crosscorrelation of the vertical and total gradients of the reduced-to-pole data. The uncertainty of that estimation is approximately 10° for each angle. Using these estimated angles, we ob-

tain an average effective susceptibility of 5×10^{-2} SI for the HK unit.

The mean and standard deviation values of the log-effective magnetic susceptibility, inclination, and declination for each rock unit are provided in Table 1. Those values define the Gaussian distributions of the magnetization parameters in a spherical coordinates system with a logarithmic distribution for magnetization amplitudes. Ideally, we would like to invert for a log-susceptibility model, but that poses challenges because the very low susceptibilities do not generate a substantial signal in the magnetic field data. Therefore, we revert to the usual practice of inverting for magnetic susceptibility on a linear scale. Our MVI algorithm inverts for each Cartesian component of magnetization $\{k_x, k_y, k_z\}$. For PGI, we need to represent the magnetization in a GMM. We thus need to obtain means and covariance matrices for $\{k_x, k_y, k_z\}$. To this end, we appeal to random numerical sampling methods. For each rock unit, we randomly sample, from their Gaussian distribution in spherical coordinates, log-effective susceptibility and angles triplets. We convert those synthetic samples to Cartesian values and use them to estimate the desired means and covariances (equations 3 and 4).

The resultant GMM for magnetic parameters can be visualized in Figure 8b. The resulting probability distributions appear elongated and tilted, indicating correlations between the Cartesian components of magnetization. Given the measured magnetization and uncertainties, the weakly magnetic PK and VK units are difficult to distinguish from a nonsusceptible background due to the nearby highly magnetic HK unit. The PK/VK unit and the background have thus been grouped under background in Figure 8b.

The resultant GMM for magnetic parameters can be visualized in Figure 8b. The resulting probability distributions appear elongated and tilted, indicating correlations between the Cartesian components of magnetization. Given the measured magnetization and uncertainties, the weakly magnetic PK and VK units are difficult to distinguish from a nonsusceptible background due to the nearby highly magnetic HK unit. The PK/VK unit and the background have thus been grouped under background in Figure 8b.

Petrophysical characterization summary

We have defined, in terms of density and magnetization, the characteristics of the background and main kimberlite units identified in the DO-27 pipe. Table 1 summarizes the quantitative values used to define the GMMs for the various inversions that we conduct. The information about a new unit, PK-minor, also is reported. This unit is used in our final inversion, and more details are given in the multiphysics PGI section.

Regarding density, the background and HK units are assigned a 0 g/cm^3 mean density contrast, whereas the PK/VK unit presents a mean density that varies with depth. The background and HK units are indistinguishable, and the

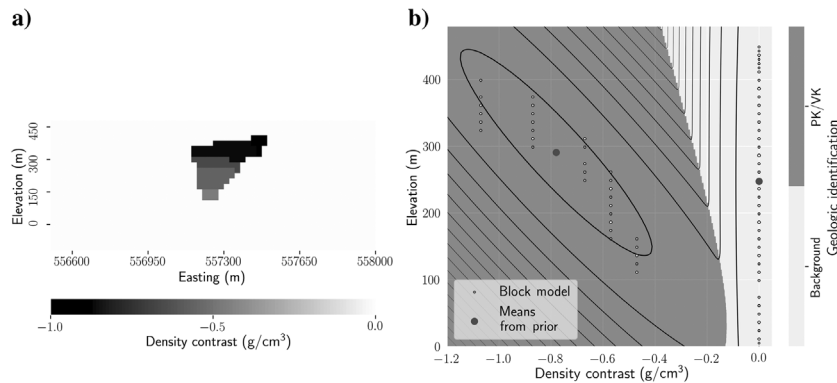


Figure 7. Design of the PK/VK unit density signature in the GMM. (a) Cross section of the density contrast estimate for the PK/VK unit from Eggleston et al. (2014) and (b) scatterplot, density contrast versus elevation of the cells, of the cross section shown in panel (a). We fit a Gaussian on each unit (PK/VK and background); the contour lines represent the isoprobability levels from the resulting GMM, and the background color indicates the geologic identification.

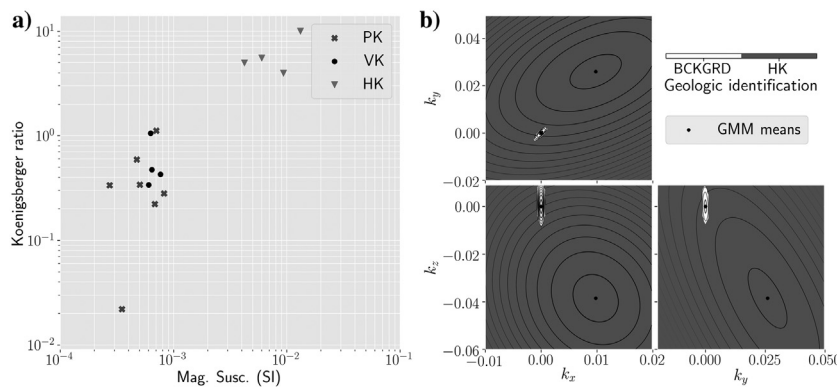


Figure 8. (a) Magnetic measurements in the laboratory and (b) 2D projections of the 3D GMM of the Cartesian components of the magnetic vector estimated for the background and HK units; the contour lines represent the isoprobability levels of the GMM, and the background color indicates the geologic identification. The background unit is limited to the space defined by the small ellipsoid.

gravity anomaly primarily is due to the PK/VK unit. Thus, carrying out an inversion just for a density contrast model with PGI requires only a petrophysical GMM consisting of two rock units (background and PK/VK).

A similar situation occurs for magnetic properties. The HK unit is dominant, and its magnetization is nearly two orders of magnitude larger than the PK/VK unit. Any inversion that focuses purely on magnetic data would have challenges delineating the PK/VK unit from the background in the presence of the HK unit. Thus, carrying out a PGI solely for a magnetic vector model only necessitates a petrophysical GMM with two rock units (background and HK).

Although only two rock units are justified when inverting for a single type of physical property, the situation changes when we consider the density and magnetic characteristics together. As illustrated in Figure 6, units that appear indistinguishable in one physical property (1D space, property 2) can be distinct when considering a higher dimensional petrophysical space (the 2D space). In our case, the background, PK/VK, and HK units are distinct in the 5D space composed of density, elevation, and the three magnetic vector components. The multiphysics inversions take advantage of that higher dimensionality of the GMM to recover all three rock units at once (see the multiphysics PGI section). We now carry out the single physics and multiphysics PGI to illustrate these ideas.

Single-physics PGIs

We now invert, with the PGI approach, data sets that are connected by a single physics. We recover a density model from gravity and gravity gradiometry data using the information that the density of the PK/VK unit increases with depth. From the magnetic data, we recover a magnetic vector model that is compatible with our knowledge about the magnetization of the HK unit. The density and magnetization models then are combined to highlight the limitation of single physics and post-inversion classification approaches in delineating the two kimberlite units.

Joint PGI of the ground gravity and Falcon airborne gravity gradiometry data

We first jointly invert the ground gravity and airborne gravity gradiometry with the addition of our petrophysical model to include our knowledge about the expected density contrasts and their variations with depth. The obtained density model is shown in Figure 9a, and it can be compared with the result obtained by jointly inverting the two data sets but without a petrophysical constraint (Figure 5). The trend with depth can be seen in the scatterplot in Figure 9b. Each survey has reached its target misfit.

A single body, reproducing the PK/VK petrophysical signature, is sufficient to fit the gravity data. The horizontal outline of this PK/VK body is in reasonable agreement with the geologic model except for a region north of the pipe. The bottom of the PK/VK body is relatively well constrained. On the north–south cross section, we can distinguish low-density material in the upper surface (approximately -0.1 g/cm^3 , at elevations greater than 300 m) that lies above the northern extension of the identified PK/VK volume. That anomaly may be related to other minor kimberlite occurrences and is still identified as background in the quasi-geology model (Figure 9b).

MVI of the airborne magnetic data with PGI

Here, we invert the magnetic data using an MVI approach to recover each component $\{k_x, k_y, k_z\}$ of a magnetic vector. The inclusion of petrophysical information through the GMM ensures that we are reproducing the signature of the HK unit.

The result of the inversion with petrophysical knowledge is shown in Figure 10a. We recover a well defined, compact magnetic body with consistent magnetic orientation reproducing the modeled petrophysical signature of HK (Figure 10b). The location of the HK unit coincides well with that obtained from drillholes, except that the eastern side of the mapped HK unit is not recovered and no dip is visible. No anomaly related to PK/VK is visible in the magnetic vector model.

Post-inversion classification of the individually obtained density and magnetic vector models

At this stage, we have obtained two physical property models. One is a density model that reproduces the gravity data sets and the PK/VK density signature. The HK unit is not necessary to explain the gravity data and is considered to be indistinguishable from the background regarding its density. The second is a magnetic

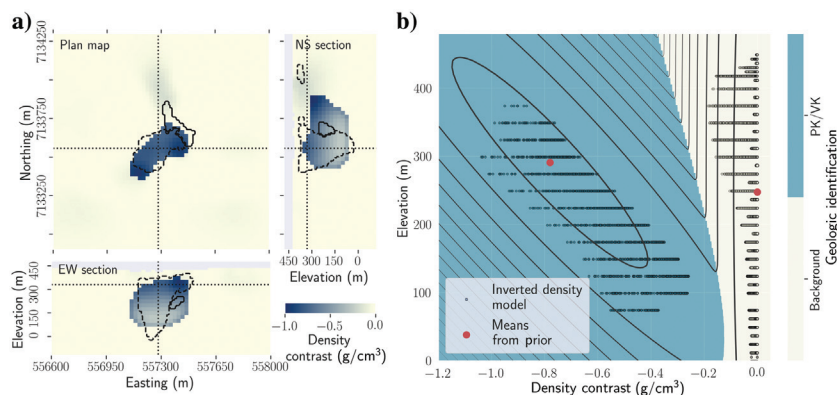


Figure 9. Inversion result with PGI of the ground gravity and Falcon surveys using the density signature of PK/VK: (a) plan map, east–west, and north–south cross sections through the recovered density contrast model along each plane (the dotted lines represent the location of each cross section) and (b) comparison between the petrophysical GMM (contour plot) used to regularize the inversion and the recovered density contrast model (scatterplot).

vector model that globally reproduces the magnetic data and HK magnetic signature. In this inversion, the PK/VK unit is deemed to be indistinguishable from the background regarding its magnetic susceptibility.

Combining the two models (Figure 11) highlights the limits of post-inversion classification with single-physics inversions of geophysical data sets. Even with the

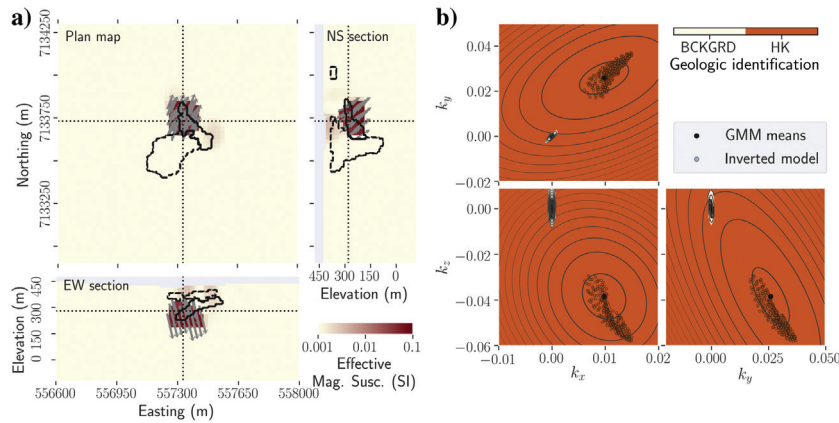


Figure 10. The result of the petrophysically guided MVI. (a) Plan map, east–west, and north–south cross sections through the magnetic vector model along each plane. The dotted lines represent the location of each cross section. The dark arrows represent the magnetization direction and strength and (b) comparison between the petrophysical GMM (contour plots) used to constrain the magnetic vector model and the recovered magnetic vector model (scatterplots). The background unit appears in the plots as the small ellipsoid. Background cells are all within that small portion of the parameters space. The geologic identification is used to color the background of the plot.

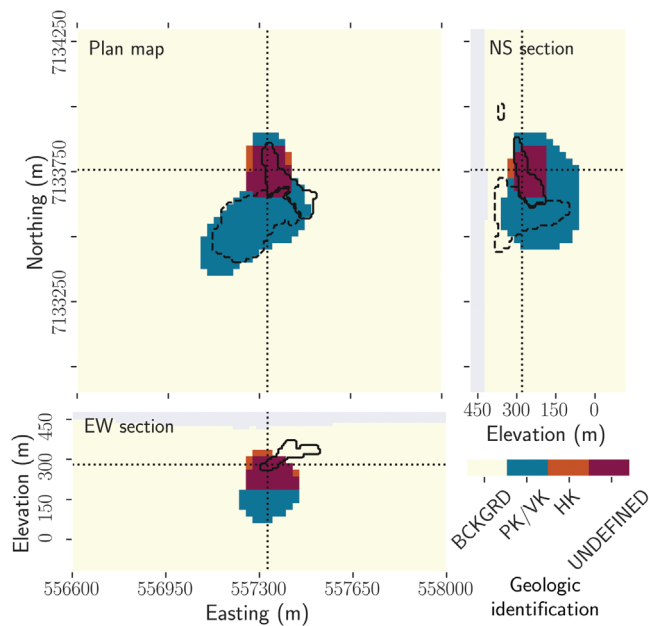


Figure 11. Plan map, east–west, and north–south cross sections through the combination of the individual PGIs. The undefined area corresponds to a volume in which the high density and magnetic contrasts were found, corresponding to no known rock unit signature. The dotted lines represent the location of each cross section.

addition of petrophysical information and the dominance of each unit in each inversion, the combination of the two models shows an important overlap between the recovered PK/VK and HK units (marked as the “undefined” area). This volume, actually covering most of the recovered HK unit, is found to have both a strong density and magnetic contrasts. This signature disagrees with our petrophysical knowledge of the area.

To overcome this, we propose to invert all three surveys (ground gravity, airborne gravity gradiometry, and airborne magnetic) together with all five coupling parameters (density contrast, elevation, and the three components of the magnetic vector).

Multiphysics PGIs

In this section, we use our PGI approach to invert all three data sets along with the petrophysical information about the rock units. We first consider three rock units (the background, PK/VK, and HK) to form the GMM. We then further refine the quasi-geology model by adding a fourth unit and geologic a priori information based on drillholes into a subsequent inversion to recover the desired geologic features.

Multiphysics inversion with petrophysical information

The multiphysics PGI result is presented in Figure 12. The improvement over the single-physics inversions, smooth and petrophysically guided, is quite pronounced. The overlapping of the units observed by combining single-physics inversions has been resolved by the multiphysics inversion, which reproduces the full 5D petrophysical distribution.

Figure 12c presents the 5D GMM by showing all possible 2D projections. The values of the physical properties model are well clustered around the prescribed means and along determined trends. The dimensionality increase of the GMM allows us to define three distinct units (the background, PK/VK, and HK), with their specific signature for all physical properties. The multiphysics inversion recovers an HK unit with a mean density contrast of approximately -0.12 g/cm^3 . Similarly, the magnetic signature of the recovered PK/VK unit now is distinguishable from the background; it has a mean effective susceptibility of $1.06 \times 10^{-3} \text{ SI}$, which is close to the expected value of $8 \times 10^{-4} \text{ SI}$. The PK/VK magnetization is oriented along the earth’s magnetic field, as required. This orientation differs from the remanent magnetization given to the HK unit. This difference in orientation can be seen in Figure 12b. It is only with the multiphysics inversion approach that we can define two clear kimberlite facies (Figure 12d).

Comparison with a geologic model from drilling

Now that we have obtained a quasi-geology model containing all three major units that reproduce the geophysical data sets and petrophysical information, we can compare it to the geologic model built from drill-holes (Figure 12d).

The HK unit is reasonably well localized, but not all of the details are reproduced by the inversion. In reality, the HK unit is a thin, dipping body that we image as a horizontal body. We miss a portion of the unit that is mapped on the east, and our unit continues further west than that in the geologic model. However, we note that few drillholes have been logged in the western area, so there might be some uncertainty in the geologic model.

The PK/VK unit, which is diamondiferous, is in good agreement with the geologic model over the region of the pipe. Importantly, the bottom extension of that unit seems to have been well constrained by incorporating the petrophysical data. The major discrepancy between our model and the geologic model is in the northern region, where some PK/VK material has been placed beneath the HK unit. This result contradicts drill results that show no PK/VK occurrence beneath the HK unit.

To understand how this happened, we need to reexamine the gravity inversion results and the information that is input into the PGI. In the inversion of the gravity data alone, low-density material is required in the region north of the pipe. However, in the magnetic inversion, that region is occupied by the HK unit, which is assumed to have no density contrast with the background. In the multiphysics inversion, any low-density material required to fit the gravity data must, therefore, be put either at depth or in a near-surface layer. However, because of the assumed dependence of density and elevation, the density of a near-surface layer must be very low. The inability to fit the gravity data with that very low-density shallow layer provides no alternative for the inversion except to put anomalous density material at depth. To resolve this inconsistency with geology, we introduce another geologic unit and carry out a new multiphysics inversion that includes expanded a priori information.

Adding geologic information into the multiphysics inversion

The previously obtained model from a multiphysics inversion with petrophysical information allows us to recover distinct units with the required petrophysical signature. However, several features of the quasi-geology model are in disagreement with the geologic knowledge from drill-

holes, namely, the northern extension of the PK/VK pipe below the HK unit and the lack of dip for the HK unit.

To overcome those issues, we revise our assumptions of what to add as a priori information into the inversion. We have assumed so far that near-surface occurrences of PK facies had similar density characteristics as the PK/VK unit found in the DO-27 pipe. Those near-surface occurrences, which showed up in the inversion results as smooth density contrast features, still were categorized as background (Figures 9 and 12). It is an indication that those minor occurrences potentially have a different petrophysical signature than the main pipe, which displays extreme density contrasts near the surface (up to approximately -1 g/cm^3). To accommodate the need to have a mass deficiency in the near-surface region north of the pipe, we introduce an additional rock unit. This new unit represents near-surface occurrences of PK-like rocks outside of the main pipe. Henceforth, we call this unit PK-minor and distinguish it from PK/VK-pipe, which has been focused on thus far, through a different density signature. We lack representative samples for PK-minor to define its petrophysical characteristics. To select its GMM param-

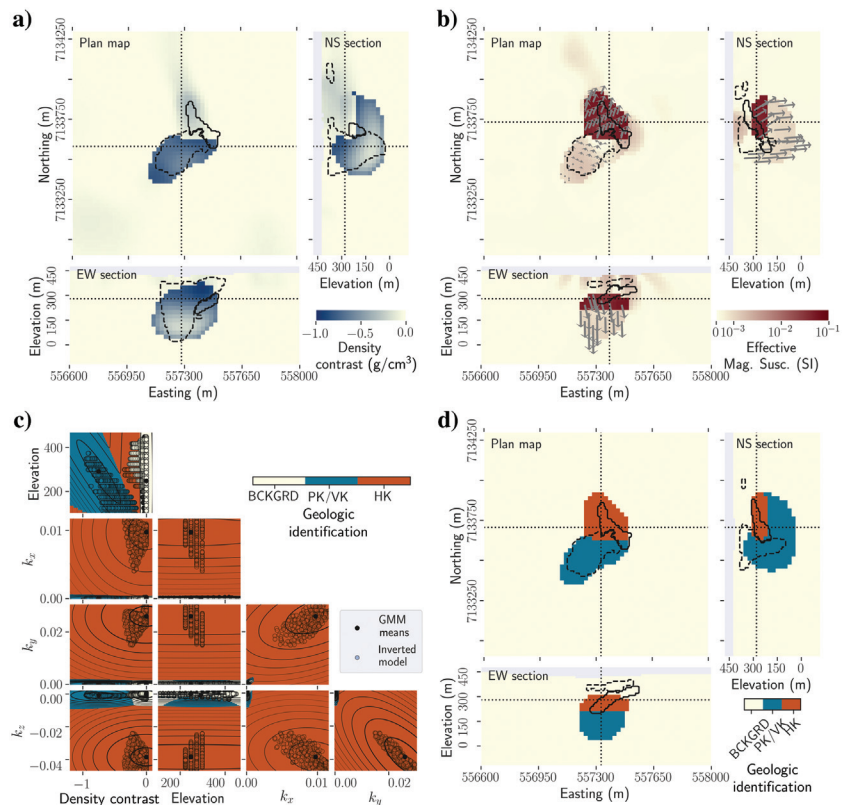


Figure 12. Results of the multiphysics PGI with three rock units. (a) Plan map: east–west, and north–south cross sections through the density contrast model. The dotted lines represent the location of each cross section. (b) Magnetic vector model: The gray arrows are the projections of the magnetization directions (unit vector) on the plane for the kimberlite units. (c) Presentation of the 5D GMM: visualization of all possible 2D projections. Comparison with the recovered model represented as the scatter plots of the four physical properties of the geophysical model and the elevation. (d) The resulting quasi-geology model from the multiphysics PGI with three rock units.

eters for the density and elevation, we ran gravity PGIs with three rock units (the background, PK/VK-pipe, and PK-minor) for a range of values for the means and standard deviations. We chose a mean density of -0.3 g/cm^3 , in line with observations in the area, with a standard deviation of 0.1 g/cm^3 , which is close to the standard deviation observed for the HK unit. The mean elevation for PK-minor is set at 360 m with a standard deviation of 10 m; those values effectively limit the occurrence of the PK-minor unit to the near surface at elevations of 300 m and greater. For its magnetic properties, we chose to assign it the same as for the main PK/VK-pipe unit. The properties of the PK-minor unit are summarized in Table 1.

In the above, we have separated the original PK/VK unit into a PK/VK-pipe and a PK-minor through distinct petrophysical signatures. These two units also are separated geographically. We include this information into the PGI by using local proportions (equation 7). We implement a simple constraint: The PK/VK-pipe unit can occur only at locations south of 7,133,685 m, which

is the northern limit of the mapped pipe, as seen in the geologic data and the geophysical inversions we ran so far. In other words, we set $\pi_{\text{PK/VK}} = 0$ at locations north of 7,133,685 m. Similarly, we set the proportions of the newly introduced PK-minor rock unit so that it occurs only north of that bound and does not overprint the surface of the pipe. It effectively decomposes our area of interest into two domains that see different GMM coupling.

The result of the multiphysics inversion with an additional rock unit for near-surface kimberlites and geologic domains is shown in Figure 13. This model is geologically appealing. It reproduces known geologic features better than in the previous multiphysics inversion. The northern extension of the PK/VK pipe unit is now gone, and the general outline of the pipe is thus much better recovered. Most of the northern tip gravity anomaly is explained by a near-surface sheet of PK-minor units, whose locations match with known occurrences in drillholes. For the HK unit, we start to obtain some sense of the dip of that unit. Its near-surface outline is again well recovered, but its thickness appears overestimated.

The introduction of the new unit also has changed how well petrophysical signatures are recovered. The density contrast of the HK unit now is closer to the null density contrast measured in samples, at an average of -0.03 g/cm^3 (compared to -0.12 g/cm^3 in the previous multiphysics inversion with three rock units). Similarly, the PK/VK-pipe unit now is very close to its measured magnetic amplitude at $8 \times 10^{-4} \text{ SI}$ (compared to $1.06 \times 10^{-3} \text{ SI}$ in the previous multiphysics inversion). The orientations of the magnetization also are consistent with the values in the GMM: they align with the earth's magnetic field for PK/VK-pipe and PK-minor and are along the remanence direction for the HK unit. The clustering of the magnetic petrophysical values of the HK unit is not as good as in previous inversions, but they still are within acceptable bounds as defined by its distribution.

The geophysical surveys are individually fit, as well as the GMM petrophysical distribution. The data misfit value of each survey, divided by its number of data, is 0.99 for the ground gravity survey, 0.84 for the airborne gravity gradiometry survey, and 0.92 for the airborne magnetic survey (targets of unity). The normalized data misfit maps are presented in Figure 14. The maps associated with gravity data are random and consistent with the assigned noise levels (Figure 14b–14d). The misfits of the

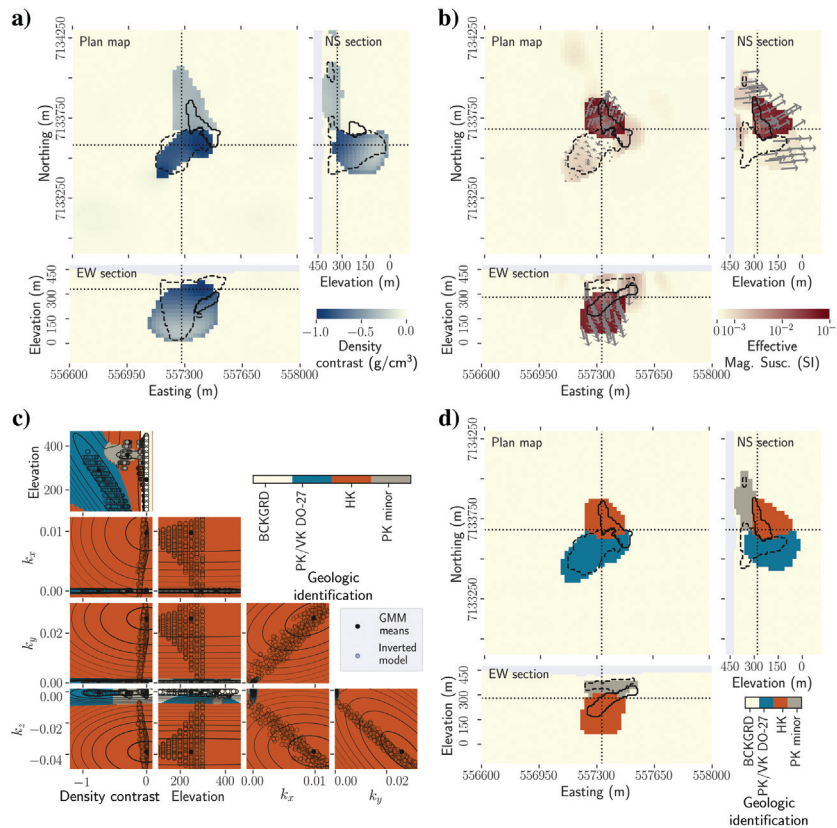


Figure 13. Results of the multiphysics PGI with an additional rock unit for near-surface PK-minor occurrences and geologic domains. (a) Plan map: east–west, and north–south cross sections through the density contrast model. The dotted lines represent the location of each cross section. (b) Magnetic vector model: the gray arrows are the projections of the magnetization directions (unit vector) on the plane for the kimberlite units. (c) Presentation of the 5D GMM: visualization of all possible 2D projections. Comparison with the recovered model represented as the scatterplots of the four physical properties of the geophysical model and the elevation. (d) The resulting quasi-geology model from the multiphysics PGI with four rock units.

airborne gravity gradiometry data (Figure 14c and 14d) appear to follow the flight path. The flight lines also are visible in the observed data (Figure 3c and 3d). For the magnetic data, even though we achieved the global geophysical target misfit, there is a coherent residual signal visible in the misfit maps (Figure 14a). The misfits are higher, up to 7 nT, just above the eastern extension of the HK body that we seem to not recover in the inversion (Figure 12b and 12d).

Discussion

The PGI framework has enabled us to jointly invert three types of geophysical data (airborne magnetic, ground gravity, and airborne gravity gradiometry) using five coupled parameters (density, elevation, and the three components of the magnetic vector). This joint approach recovers a final quasi-geology model that maps all expected geologic units (the background, PK/VK-pipe, HK, and PK-minor units) by reproducing their petrophysical characteristics in the inversion. This result is unobtainable by inverting data sets separately and then carrying out a post-inversion classification of the recovered physical properties.

For this study, we have drillhole information, and we built a geologic model from it to compare with our results. For DO-27, the PK unit is the diamondiferous kimberlite unit, and so estimating its volume and shape is a key for resource estimation. Although PK is indistinguishable from VK from the potential-fields data, VK has a negligible volume in the geologic model compared to PK. Therefore, we can interpret the PK/VK-pipe unit as representing the diamondiferous PK unit. Reproducing the PK density signature, with its depth dependence, allows us to obtain an informed estimation of its shape and volume. The surface outline and bottom extension of the potentially diamondiferous unit are in good agreement with the geologic model, but the quasi-geology model is more rounded at depth. The estimated volume of the PK/VK-pipe is evaluated at $28 \times 10^6 \text{ m}^3$ and can be compared to $15.7 \times 10^6 \text{ m}^3$, obtained from the geologic model (see Harder et al. [2009] and Figure 12d). Most of the volume discrepancy is concentrated at depth, where the gravity surveys are less sensitive.

From a numerical perspective, the MVI problem with petrophysical information has been more challenging than the gravity inversions. This is due in part to the orders of magnitude difference between the various units, the challenge of inverting for logarithmically distributed effective susceptibilities, and the lack of oriented samples to determine the magnetic characteristics of the HK unit. In principle, the use of MVI in spherical coordinates seems desirable,

but the additional nonlinear transformations complicate an already challenging problem. Therefore, we have implemented the Cartesian formulation. Nevertheless, we still were able to recover a unit with the identified magnetic signature of HK. Realistically, however, the geology probably is more complicated than we have modeled. Assuming a single and relatively uniform HK unit is likely insufficient to explain the whole magnetic data, as shown by the data misfit map in Figure 14a. During our study, we tried to obtain various estimates of the orientation of the remanent field, such as using a sparse MVI code in spherical coordinates (Fournier and Oldenburg, 2019) or obtaining the best-fitting amplitude and angles for the available shape of HK in the geologic model. Although the recovered inclinations appeared consistent across estimations with the value obtained in Devriese et al. (2017), the declinations spanned a wide range. Those challenges could be explored in a future case study. Although the inversion results seem to validate the current petrophysical estimates, the estimation of the density, magnetic susceptibility, and remanent magnetization orientation of the HK unit could be significantly improved by measuring new, oriented samples.

Finally, although we used local proportions to implement elementary geologic expectations, a complete inclusion of all the drillhole information is yet to be done. It could help further refine the quasi-geology model, such as narrowing the PK/VK pipe unit at depth or constraining the thickness of the HK unit. The inclusion and extrapolation of drillhole information within the PGI framework is part of our current research.

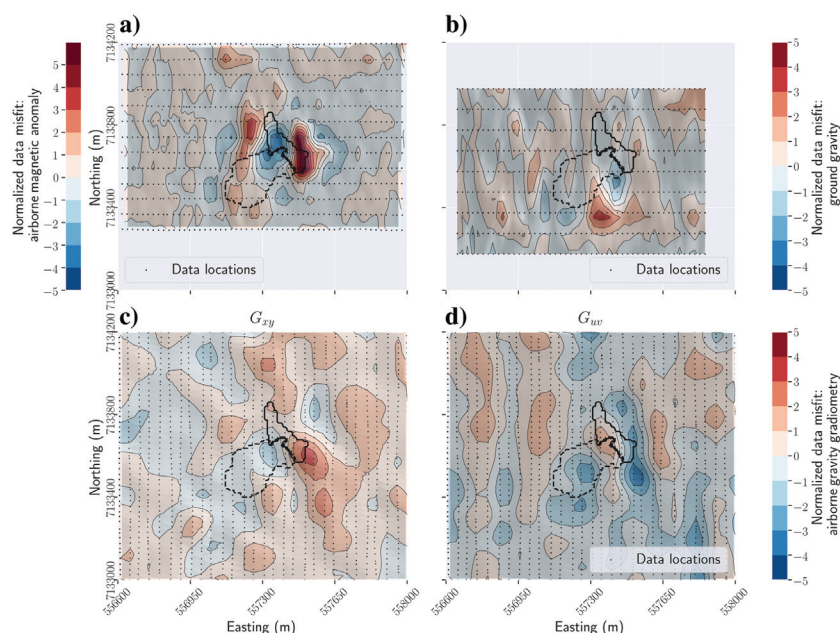


Figure 14. Normalized data misfits for all the data sets from the multiphysics PGI with geologic domains and four rock units. (a) For the magnetic data, (b) for the gravity data, and (c) and (d) for the gravity gradiometry data.

Conclusion

Inferences from inversions of single data sets, even when they are input into post-inversion classification algorithms, can be deficient. This limitation is a motivation to carry out joint inversions. The challenge is how to link the data sets together, in a practical sense, and how to include other relevant information. We adopt the PGI framework to use petrophysical measurements as the linkage and apply it to the field data acquired over the DO-27 kimberlite pipe. We have successfully jointly inverted airborne gradiometry, ground gravity, and airborne magnetic data, along with measured physical properties and geologic information. Our framework outputs physical property models and a quasi-geology model. The results that include multiple physics, coupled with petrophysical and geologic information, are shown to better resolve and distinguish the rock unit bodies compared to interpreting single-physics inversion results. The fact that we can fit all of the geophysical data sets while reproducing the petrophysical signatures, such as varying densities with depth and magnetization orientations, is a significant achievement. Working with a complex geologic model presents challenges, and the flexibility of the PGI framework offers multiple ways to tackle them. Refining the classification of rock units, testing for various petrophysical signatures, and defining local geologic information to satisfy the field observations have been keys to recover a satisfying quasi-geology model. Nevertheless, further refinements of our PGI implementation could improve the estimate of the volumes and structures of the PK and HK units. Such refinements could include a more extensive integration of the drillhole information and address the complexity of the magnetization signatures. Moreover, there are other geophysical data sets that can provide constraints on the electromagnetic properties of the rock units, and incorporating those can further reduce the discrepancies between our geophysical and geologic models. The DO-27 kimberlite pipe presents an ideal test site on which to test these procedures.

Acknowledgments

The authors thank K. Witherly and J. Jansen for the inspiring discussions about the DO-18/DO-27 data sets over the past 15 years. We also would like to thank R. Enkin and D. Cowan for the insightful conversations about the measurements of petrophysical properties. We sincerely thank Condor Consulting Inc., Peregrine Diamonds Ltd., and Kennecott for making the data sets available for our research. Finally, we want to acknowledge the work of the SimPEG community, without which this study would not have been possible, and especially L. J. Heagy for the development of tools to mix and add together objective functions and J. Capriotti for the development of a fast octree mesh.

Data and materials availability

Data associated with this research are confidential and cannot be released.

References

- Astic, T., L. J. Heagy, and D. W. Oldenburg, 2020, Petrophysically and geologically guided multi-physics inversion using a dynamic Gaussian mixture model: *Geophysical Journal International*, doi: [10.1093/gji/ggaa378](https://doi.org/10.1093/gji/ggaa378).
- Astic, T., and D. W. Oldenburg, 2019, A framework for petrophysically and geologically guided geophysical inversion using a dynamic Gaussian mixture model prior: *Geophysical Journal International*, **219**, 1989–2012, doi: [10.1093/gji/ggz389](https://doi.org/10.1093/gji/ggz389).
- Cockett, R., S. Kang, L. J. Heagy, A. Pidlisecky, and D. W. Oldenburg, 2015, SimPEG: An open source framework for simulation and gradient based parameter estimation in geophysical applications: *Computers and Geosciences*, **85**, 142–154, doi: [10.1016/j.cageo.2015.09.015](https://doi.org/10.1016/j.cageo.2015.09.015).
- Dempster, A. P., N. M. Laird, and D. B. Rubin, 1977, Maximum likelihood from incomplete data via the EM algorithm: *Journal of the Royal Statistical Society, Series B*, **39**, 1–38, doi: [10.1111/j.2517-6161.1977.tb01600.x](https://doi.org/10.1111/j.2517-6161.1977.tb01600.x).
- Devriese, S. G. R., K. Davis, and D. W. Oldenburg, 2017, Inversion of airborne geophysics over the DO-27/DO-18 kimberlites — Part 1: Potential fields: Interpretation, **5**, no. 3, T299–T311, doi: [10.1190/INT-2016-0142.1](https://doi.org/10.1190/INT-2016-0142.1).
- Doyle, B. J., K. Kivi, and B. H. S. Smith, 1998, The Tli Kwi Cho (DO27 and DO18) diamondiferous kimberlite complex, Northwest Territories: Proceedings of the 7th International Kimberlite Conference, 194–204, doi: [10.29173/ikc2682](https://doi.org/10.29173/ikc2682).
- Dyke, A., and V. Prest, 1987, Late Wisconsinan and Holocene history of the Laurentide ice sheet: *Géographie physique et Quaternaire*, **41**, 237–263, doi: [10.7202/032681ar](https://doi.org/10.7202/032681ar).
- Eggleston, T., K. Brisebois, and J. Pell, 2014, Lac de Gras project northwest territories, Canada: Technical Report NI 43-101, Peregrine Diamonds Ltd.
- Enkin, R. J., T. S. Hamilton, and W. A. Morris, 2020, The Henkel Petrophysical plot: Mineralogy and lithology from physical properties: *Geochemistry, Geophysics, Geosystems*, **21**, e2019GC008818, doi: [10.1029/2019GC008818](https://doi.org/10.1029/2019GC008818).
- Field, M., and B. H. S. Smith, 1998, Textural and genetic classification schemes for kimberlite: A new perspective: Proceedings of the 7th International Kimberlite Conference, Extended Abstracts, 214–216.
- Fournier, D., S. Kang, M. S. McMillan, and D. W. Oldenburg, 2017, Inversion of airborne geophysics over the DO-27/DO-18 kimberlites — Part 2: Electromagnetics: Interpretation, **5**, no. 3, T313–T325, doi: [10.1190/INT-2016-0140.1](https://doi.org/10.1190/INT-2016-0140.1).
- Fournier, D., and D. W. Oldenburg, 2019, Inversion using spatially variable mixed Lp-norms: *Geophysical Journal International*, **218**, 268–282, doi: [10.1093/gji/ggz156](https://doi.org/10.1093/gji/ggz156).
- Giraud, J., E. Pakyuz-Charrier, M. Jessell, M. Lindsay, R. Martin, and V. Ogarko, 2017, Uncertainty reduction in joint inversion using geologically conditioned petrophysical constraints: *Geophysics*, **82**, no. 6, ID19–ID34, doi: [10.1190/geo2016-0615.1](https://doi.org/10.1190/geo2016-0615.1).
- Giuseppe, M. G. D., A. Troiano, C. Troise, and G. D. Natale, 2014, k-Means clustering as tool for multivariate geo-

- physical data analysis. An application to shallow fault zone imaging: *Journal of Applied Geophysics*, **101**, 108–115, doi: [10.1016/j.jappgeo.2013.12.004](https://doi.org/10.1016/j.jappgeo.2013.12.004).
- Harder, M., B. S. Smith, C. Hetman, and J. Pell, 2009, The evolution of geological models for the DO-27 kimberlite, NWT, Canada: Implications for evaluation: *Lithos*, **112**, 61–72, doi: [10.1016/j.lithos.2009.06.024](https://doi.org/10.1016/j.lithos.2009.06.024).
- Jansen, J., and K. Witherly, 2004, The Tli Kwi Cho kimberlite complex, Northwest Territories, Canada: A geophysical case study: 74th Annual International Meeting, SEG, Expanded Abstracts, 1147–1150, doi: [10.1190/1.1839654](https://doi.org/10.1190/1.1839654).
- Kadiyala, K. R., and K. S. R. Murthy, 1977, Estimation of regression equation with Cauchy disturbances: *The Canadian Journal of Statistics/La Revue Canadienne de Statistique*, **5**, 111–120, doi: [10.2307/3315088](https://doi.org/10.2307/3315088).
- Kang, S., D. Fournier, and D. W. Oldenburg, 2017, Inversion of airborne geophysics over the DO-27/DO-18 kimberlites — Part 3: Induced polarization: *Interpretation*, **5**, no. 3, T327–T340, doi: [10.1190/INT-2016-0141.1](https://doi.org/10.1190/INT-2016-0141.1).
- Keating, P., and P. Sailhac, 2004, Use of the analytic signal to identify magnetic anomalies due to kimberlite pipes: *Geophysics*, **69**, 180–190, doi: [10.1190/1.1649386](https://doi.org/10.1190/1.1649386).
- Kjarsgaard, B., and A. Levinson, 2002, Diamonds in Canada: *Gems and Gemology*, **38**, 208–238, doi: [10.5741/GEMS.38.3.208](https://doi.org/10.5741/GEMS.38.3.208).
- Kjarsgaard, B. A., 2007, Kimberlite pipe models: Significance for exploration: *Proceedings of Exploration 07: Fifth Decennial International Conference on Mineral Exploration*, 667–677.
- Koenigsberger, J. G., 1938, Natural residual magnetism of eruptive rocks: *Terrestrial Magnetism and Atmospheric Electricity*, **43**, 299–320, doi: [10.1029/TE043i003p00299](https://doi.org/10.1029/TE043i003p00299).
- Latham, A. G., K. L. Harding, P. Lapointe, W. A. Morris, and S. J. Balch, 1989, On the lognormal distribution of oxides in igneous rocks, using magnetic susceptibility as a proxy for oxide mineral concentration: *Geophysical Journal International*, **96**, 179–184, doi: [10.1111/j.1365-246X.1989.tb05259.x](https://doi.org/10.1111/j.1365-246X.1989.tb05259.x).
- Lee, J. B., 2001, Falcon gravity gradiometer technology: *Exploration Geophysics*, **32**, 247–250, doi: [10.1071/EG01247](https://doi.org/10.1071/EG01247).
- Lelièvre, P. G., and D. W. Oldenburg, 2009, A 3D total magnetization inversion applicable when significant, complicated remanence is present: *Geophysics*, **74**, no. 3, L21–L30, doi: [10.1190/1.3103249](https://doi.org/10.1190/1.3103249).
- Li, Y., 2005, 3-D inversion of gravity gradiometer data: 75th Annual International Meeting, SEG, Expanded Abstracts, 1470–1473, doi: [10.1190/1.1816383](https://doi.org/10.1190/1.1816383).
- Li, Y., A. Melo, C. Martinez, and J. Sun, 2019, Geology differentiation: A new frontier in quantitative geophysical interpretation in mineral exploration: *The Leading Edge*, **38**, 60–66, doi: [10.1190/tle38010060.1](https://doi.org/10.1190/tle38010060.1).
- Li, Y., and D. W. Oldenburg, 1996, 3-D inversion of magnetic data: *Geophysics*, **61**, 394–408, doi: [10.1190/1.1443968](https://doi.org/10.1190/1.1443968).
- Li, Y., and D. W. Oldenburg, 1998, 3-D inversion of gravity data: *Geophysics*, **63**, 109–119, doi: [10.1190/1.1444302](https://doi.org/10.1190/1.1444302).
- Macnae, J., 1995, Applications of geophysics for the detection and exploration of kimberlites and lamproites: *Journal of Geochemical Exploration*, **53**, 213–243, doi: [10.1016/0375-6742\(94\)00057-1](https://doi.org/10.1016/0375-6742(94)00057-1).
- Martinez, C., and Y. Li, 2015, Lithologic characterization using airborne gravity gradient and aeromagnetic data for mineral exploration: A case study in the Quadrilátero Ferrífero, Brazil: *Interpretation*, **3**, no. 2, SL1–SL13, doi: [10.1190/INT-2014-0195.1](https://doi.org/10.1190/INT-2014-0195.1).
- Melo, A. T., J. Sun, and Y. Li, 2017, Geophysical inversions applied to 3D geology characterization of an iron oxide copper-gold deposit in Brazil: *Geophysics*, **82**, no. 5, K1–K13, doi: [10.1190/geo2016-0490.1](https://doi.org/10.1190/geo2016-0490.1).
- Murphy, K. P., 2012, *Machine learning: A probabilistic perspective*: The MIT Press.
- Oldenburg, D. W., and Y. Li, 2005, Inversion for applied geophysics: A tutorial, *in* D. K. Butler, ed., *Near-surface geophysics*: SEG, **5**, 89–150, doi: [10.1190/1.9781560801719.ch5](https://doi.org/10.1190/1.9781560801719.ch5).
- Oldenburg, D. W., Y. Li, and R. G. Ellis, 1997, Inversion of geophysical data over a copper gold porphyry deposit: A case history for Mt. Milligan: *Geophysics*, **62**, 1419–1431, doi: [10.1190/1.1444246](https://doi.org/10.1190/1.1444246).
- Paasche, H., 2016, Post-inversion integration of disparate tomographic models by model structure analyses, *in* integrated imaging of the earth: *American Geophysical Union*, **5**, 69–91, doi: [10.1002/9781118929063.ch5](https://doi.org/10.1002/9781118929063.ch5).
- Paasche, H., J. Tronicke, K. Holliger, A. G. Green, and H. Maurer, 2006, Integration of diverse physical-property models: Subsurface zonation and petrophysical parameter estimation based on fuzzy c-means cluster analyses: *Geophysics*, **71**, no. 3, H33–H44, doi: [10.1190/1.2192927](https://doi.org/10.1190/1.2192927).
- Parker, R. L., 1977, Understanding inverse theory: *Annual Review of Earth and Planetary Sciences*, **5**, 35–64, doi: [10.1146/annurev.ea.05.050177.000343](https://doi.org/10.1146/annurev.ea.05.050177.000343).
- Pawlowski, B., 1998, Gravity gradiometry in resource exploration: *The Leading Edge*, **17**, 51–52, doi: [10.1190/1.1437820](https://doi.org/10.1190/1.1437820).
- Power, M., and D. Hildes, 2007, Geophysical strategies for kimberlite exploration in northern Canada: *Proceedings of Exploration '07: Fifth Decennial International Conference on Mineral Exploration*, 1025–1031.
- Rauen, A., H. C. Soffel, and H. Winter, 2000, Statistical analysis and origin of the magnetic susceptibility of drill cuttings from the 9.1-km-deep KTB drill hole: *Geophysical Journal International*, **142**, 83–94, doi: [10.1046/j.1365-246x.2000.00141.x](https://doi.org/10.1046/j.1365-246x.2000.00141.x).
- Witherly, K., 2005, Report on VTEM test program over three kimberlites, Lac de Gras area, Northwest Territories, Canada: Technical Report, Condor Consulting.



Thibaut Astic received an M.S. (2011) in geological engineering from the École Nationale Supérieure des Mines de Nancy (France) and an M.S. (2012) in applied geophysics from the École Polytechnique de Montréal (Québec, Canada). He is currently a Ph.D. candidate at the Geophysical Inversion Facility (GIF) at the University of British Columbia (UBC, Canada; program's end in 2020). He worked as a junior engineer at the Quebec Department of Natural Resources and at geophysical data acquisition and processing companies (Quantec Geosciences Ltd., Novatem Inc.). His research focuses on joint inversion coupled by petrophysical and geologic information and developing open-source tools for the geosciences community, mostly through the Python package SimPEG.



Dominique Fournier received a B.S. (2012), an M.S. (2015), and a Ph.D. (2019) in geophysics from the University of British Columbia. He works as a scientific programmer at Mira Geoscience Ltd. His research focuses on nonlinear inverse problems applied to base metal exploration.



Doug Oldenburg received a B.S. (1967) in physics and an M.S. (1969) in geophysics from the University of Alberta in Edmonton and a Ph.D. (1974) in earth sciences from UCSD. After a three-year postdoc in Alberta, he joined the Geophysics and Astronomy Department at the University of British Columbia. He remains at UBC, where he is currently a professor, director of the Geophysical Inversion Facility (UBC-GIF), and holder of the TeckCominco Senior Keevil Chair in Mineral Exploration. He is an honorary member of CSEG and SEG. His 40-year research career has focused on the development of inversion methodologies and their application in solving applied problems. He, with students and colleagues at UBC-GIF, has developed forward modeling and inversion algorithms for seismic, gravity, magnetic, and electromagnetic data. His current research interests include 3D forward inversion of EM data, development of software for unexploded ordnance discrimination, and the use of self potentials for dam safety investigations. He has presented the SEG 2017 DISC, "Geophysical Electromagnetics: Fundamentals and Applications."